J. Plasma Physics (199X), *vol.* 00, *part* 0, *pp.* 1–000. Printed in the United Kingdom 1

Comparisons of current-voltage and energy flux relationships based on O- and U-shaped potential models

P. JANHUNEN[1] and A. OLSSON[2,1]

[1] Finnish Meteorological Institute, Geophysical Research, Helsinki, Finland.

[2] Swedish Institute of Space Physics, Uppsala Division, Uppsala, Sweden.

(Received 20 May 1999)

Recent statistical studies using electric field measurements at 4 Earth radii altitude suggest that the low-altitude U-shaped potential contours must close below 4 R_E altitude, thus forming an O-shaped potential. We derive the current-voltage and energy flux relationships based on an O-shaped potential model and compare the results with the classical current-voltage and energy flux relationships which are based on the U-shaped potential model. We derive the current-voltage and energy flux relationships taking into account magnetospheric electrons for the Maxwellian and kappa source plasma distribution functions. From earlier statistical studies it follows that the source plasma temperature T is roughly proportional to the peak energy U. We discuss the implications of this in both current density and energy flux based on O- and U-shaped potentials, respectively. With the assumption $T \sim U$ the current density depends on the square root of U and the energy flux on $U^{3/2}$ for both U-shaped and O-shaped case. In this sense, the often-quoted linear current-voltage relationship does not really exist.

1. Introduction

For a long time, U-shaped potential contours (Figure 1, *Carlqvist and Boström,* 1970) have been suggested to explain the auroral acceleration and the shape of the inverted-V spectra (for a recent review, see *Bryant,* 1999). However, in a recent statistical study using Polar satellite data at about 4 Earth radii (R_E) altitude we failed to find the expected convergent electric field signatures that should inescapably be associated with the "upright legs" of a U-shaped potential (*Janhunen et al.,* 1998a), and an O-shaped potential (Figure 2) was suggested as an alternative. Notice that by definition, potential contours must always close somewhere, even if only in the opposite hemisphere, but here we use the term "O-shaped potential" to describe a situation where the potential contours close rather close to the ionosphere, below about 4 R_E altitude. Afterwards we have found evidence for electrostatic wave activity and simultaneous parallel acceleration at the same altitude, which may provide a self-consistent mechanism to maintain such a potential structure; these findings will be published elsewhere.

From the theoretical point of view, if O-shaped potentials exist in the Earth's magnetosphere at 2-4 R_E altitude, the first thing to know before addressing self-consistency is how individual charged particles (we are mostly interested in elec-

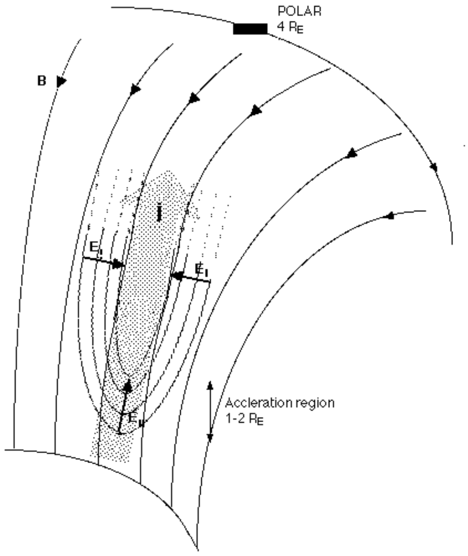

Figure 1. A schematic figure of a U-shaped potential drop.

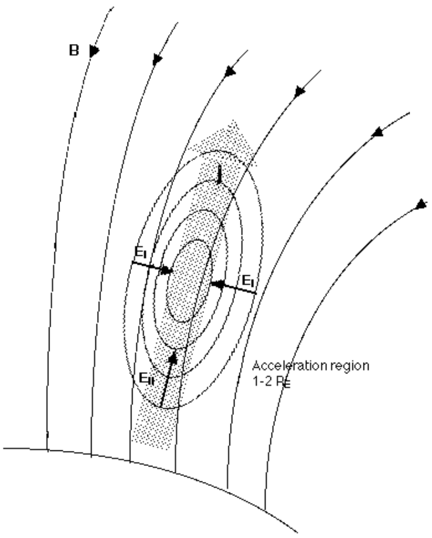

Figure 2. A schematic figure of an O-shaped potential well.

trons) move in such a potential structure, in the absence of wave-particle interactions, when a strong dipolar magnetic field persists. In previous works, formulas for the current density and energy flux have been derived for a U-shaped potential drop (*Knight,* 1973, *Lemaire and Scherer,* 1973, *Lemaire and Scherer,* 1978, *Lundin and Sandahl,* 1978, *Fridman and Lemaire,* 1980, *Lemaire and Scherer,* 1983, *Janhunen and Olsson,* 1998).

Assuming adiabatic motion (i.e., neglecting wave-particle interactions), an O-shaped negative potential barrier acts as a high-pass filter for precipitating electrons. The usually observed inverted-V type differential flux energy spectra can at least qualitatively be explained by an O-shaped potential equally well as by a U-shaped one, provided that the phase space density of magnetospheric electrons is high enough in the loss cone.

The purpose of this paper is to derive expressions for the current density and energy flux for the case when magnetospheric electrons pass through an O-shaped potential and compare it with corresponding formulas in the U-shaped model. We first derive general formulas applicable to any source plasma distribution function. We then apply our methods to Maxwellian and kappa distributions, comparing the results. A similar presentation can be seen in *Janhunen and Olsson,* 1998 for the case of U-shaped potential drop model. The kappa distribution is expected to model the distribution function better than the Maxwellian in situations where the distribution has a high energy tail.

We show that the exact nonlinear current density and energy flux formulas can be approximated in almost all practical situations by linearization with respect to the small quantity $B(src)/B(i)$, where $B(src)$ and $B(i)$ are the equatorial magnetospheric (at the source plasma region) and ionospheric magnetic fields, respectively. This result is in line with earlier calculations made in a U-shaped geometry (*Janhunen and Olsson,* 1998).

2. Theory

We will first find general expressions for the current density and energy flux for arbitrary source plasma distributions in the case of an O-shaped potential. Our initial treatment is rather similar to *Janhunen and Olsson* (1998).

We consider an isotropic Maxwellian distribution, given by

$$f_M(W_\parallel, W_\perp) = N_e \left(\frac{m}{2\pi T}\right)^{3/2} \exp\left(-\frac{W_\parallel + W_\perp}{T}\right). \tag{2.1}$$

We will also need the kappa distribution function, which is given by

$$f_\kappa(W_\parallel, W_\perp) = N_e \left(\frac{m}{2\pi\kappa T}\right)^{3/2} \frac{\Gamma(\kappa+1)}{\Gamma(\kappa-1/2)} \left(1 + \frac{W_\parallel + W_\perp}{\kappa T}\right)^{-(\kappa+1)}. \tag{2.2}$$

(*Vasyliunas,* 1968). In these formulas, Γ is the Euler Gamma function, N_e is the source plasma density (in the magnetosphere), $W_\parallel$ and $W_\perp$ are the parallel and perpendicular particle kinetic energies, m is the particle mass (in practice, the electron mass), T is the source plasma isotropic temperature in energy units and κ is the parameter characterizing the kappa distribution (the power-law spectral index). Actually, if the true temperature T_κ^{true} of the kappa distribution plasma is defined in terms of the total energy density, it becomes $T_\kappa^{\mathrm{true}} = \kappa T/(\kappa - 3/2)$ (*Collier,* 1995), where T is the parameter appearing in Equation (2.2). We choose to write our formulas in terms of T rather than T_κ^{true}.

Distributions (2.1) and (2.2) are given in energy variables and are normalized to the particle number density N_e as

$$2\pi \int_0^\infty \int_0^\infty f(W_\|, W_\perp) \sqrt{\frac{2}{m^3 W_\|}} dW_\| dW_\perp = N_e. \tag{2.3}$$

where f stands for either f_M or f_κ.

The current density can be computed from the normalization integral [Equation (2.3) by multiplying with the factor $ev_\|$ and reducing the domain of integration (see below). To get the current density at the ionospheric plane it has to be multiplied by the factor $(B(i)/B(src))$ where $B(i)$ and $B(src)$ are the magnetic field strengths at the ionosphere and at the magnetospheric source plasma region, respectively. To account for the field-aligned current (FAC) in one hemisphere only, the factor $(1/2)$ has to be added. Further, assumptions of hot magnetospheric electrons, neglection of gravitation, a maxwellian source plasma which is continously replenished are also made and are the same limitations as those in the derivation of the current density based on a U-shaped potential model (*Fridman and Lemaire,* 1980, *Janhunen and Olsson,* 1998):

$$j = 2\pi e \left(\frac{1}{2}\right) \left(\frac{B(i)}{B(src)}\right) \int_{W_\|^{\min}}^{W_\|^{\max}} dW_\| \int_0^{W_\perp^{\max}} dW_\perp f(W_\|, W_\perp) \sqrt{\frac{2}{m^3 W_\|}} v_\| \tag{2.4}$$

where $v_\| = \sqrt{2W_\|/m}$. See further below the values of the integrands $W_\|^{\min}$, $W_\|^{\max}$, $W_\perp^{\max}$.

Equation (2.4) is apart from the integration domain the same as the one computed from *Fridman and Lemaire* (1980) which is based on the U-shaped potential model.

The integration domains for the current density based on U-and O-shaped potential models, respectively are a result of the conservation of the first adiabatic invariant and the total energy, which give

$$W_\|(s) = W_\|(src) - W_\perp(src)(b_s - 1) - U(s) \tag{2.5}$$

where $W_\|(s)$ is the parallel energy of an electron in position s along the flux tube and $U(s)$ is the potential energy, which is assumed to be zero at the ionospheric level and non-negative everywhere. In the case of the O-shaped potential $U(src) = 0$ as well. b_s is short for $B(s)/B(src)$ where src stands for the source plasma region in the magnetospheric eqatorial plane. The ratio $B(i)/B(src)$ will be referred to as b_i.

For precipitating electrons $W_\|(s)$ must be non-negative and from (2.5) we get the condition

$$W_\|(src) \geqslant W_\perp(src)\,(b_s - 1) + U(s) \tag{2.6}$$

This condition should hold at every point, i.e. for all s.

The task is now to compute the lower $W_\|$ integration limit $W_\|^{\min}$ which must be found by maximising (2.6) with respect to s:

$$W_\|^{\min} = \max_s \left[W_\perp(src)(b_s - 1) + U(s)\right] \tag{2.7}$$

The maximum of this function occurs either at the ionospheric endpoint or somewhere along the flux tube where the derivative is zero. At the ionospheric endpoint

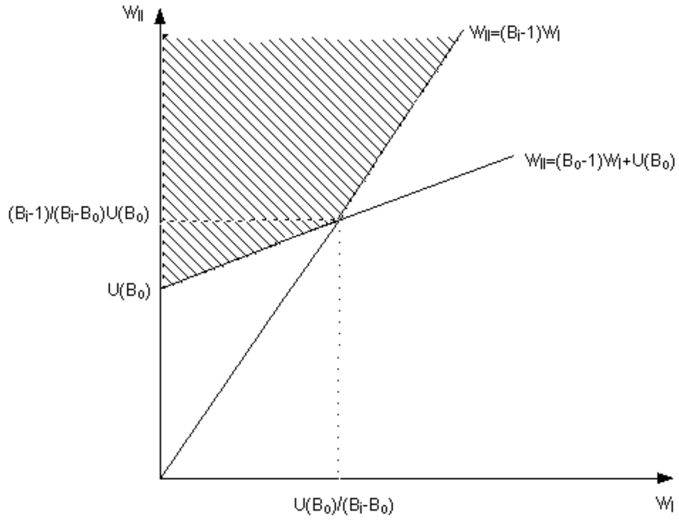

Figure 3. Parallel versus perpendicular electron energy. Particles with energy and pitch angle in the hatched area will precipitate. Integration over the two hatched domains is needed to get the current density.

we get

$$W_{\parallel}^{\min} \geqslant W_{\perp}(src)\,(b_i - 1)\,. \tag{2.8}$$

Putting the derivative equal to zero one obtains

$$W_{\perp}(src) + \frac{\partial U}{\partial b_s} = 0. \tag{2.9}$$

To solve equation (2.9) for b_s we assume that the term $W_{\perp}(src)$ can be neglected. Then the function attains its maximum at the same place where U maximizes, i.e. at the center of the O-shaped potential which we denote by b_o. The justification is as follows. From (2.8) it follows that $W_{\perp}(src) \leqslant W_{\parallel}(src)/(b_i - 1)$. Typically $W_{\parallel} \sim U$. Also, the center of the O-shaped potential is at 2-4 R_E altitude whence $b_i \gg b_o$. Thus we obtain $W_{\perp}(src) \ll U/b_o \sim \partial U/\partial b_s$, which shows that dropping the $W_{\perp}(src)$ term does not much affect the location of the maximum.

We thus get the condition

$$W_{\parallel}^{\min} \geqslant W_{\perp}(src)\,(b_o - 1) + U(b_o) \tag{2.10}$$

In Figure 3 every point in the hatched area corresponds to an electron orbit. The limiting conditions for electrons that will precipitate are marked and it is seen that two integration domains are needed for evaluating the current density,

$$j = \frac{2\pi e}{m^2} b_i$$

$$\left(\int_{U(b_o)}^{\frac{b_i-1}{b_i-b_o}U(b_o)} dW_\parallel \int_0^{\frac{W_\parallel - U(b_o)}{b_o-1}} dW_\perp f(W_\parallel, W_\perp) + \int_{\frac{b_i-1}{b_i-b_o}U(b_o)}^{\infty} dW_\parallel \int_0^{\frac{W_\parallel}{b_i-1}} dW_\perp f(W_\parallel, W_\perp) \right) \tag{2.11}$$

The formula for the energy flux ε is similar Eq.(2.11) except that now we drop the e and include $W_\parallel + W_\perp$ in the integrands:

$$\varepsilon = \frac{2\pi}{m^2} b_i \left(\int_{U(b_o)}^{\frac{b_i-1}{b_i-b_o}U(b_o)} dW_\parallel \int_0^{\frac{W_\parallel - U(b_o)}{b_o-1}} dW_\perp f(W_\parallel, W_\perp)(W_\parallel + W_\perp) + \int_{\frac{b_i-1}{b_i-b_o}U(b_o)}^{\infty} dW_\parallel \int_0^{\frac{W_\parallel}{b_i-1}} dW_\perp f(W_\parallel, W_\perp)(W_\parallel + W_\perp) \right). \tag{2.12}$$

2.1. Maxwellian distribution

We will now derive the exact and approximate current density and energy flux formulas for the Maxwellian distribution for an O-shaped potential case. We will then compare the resulting formulas with previous results for the U-shaped potential.

2.1.1. Maxwellian current density. For the Maxwellian distribution (2.1) the general current density formula (2.11) yields

$$j^{M,O} = eN_e \sqrt{\frac{T}{2\pi m}} \frac{1}{b_o} \exp\left(\frac{-U}{T}\right) \left(b_i + (b_o - b_i) \exp\left(\frac{b_o U}{-b_i T + b_o T}\right)\right) \tag{2.13}$$

This expression can be much simplified by invoking the approximation $b_i \gg 1$ ($B(i) \gg B(src)$). A straightforward series expansion of (2.13) yields

$$j^{M,O}_{\text{Appr.}} = \frac{eN_e}{\sqrt{2\pi m T}} \exp\left(\frac{-U}{T}\right)(T + U)\,. \tag{2.14}$$

Often the temperature has been assumed to be constant in the current-voltage relationship, but actually an approximately linear relationship has been found to exist between the temperature and the peak energy (*Lin and Hoffman, 1979*).

Olsson et al. (1998) gathered in their Table 1 various average parameters, including the temperature and the peak energy, from different studies. In Figure 4 we show the relation between the temperature and the peak energy based on this table, together with a fitted line. The equation of the fit is $T = T_0 + 0.31U$ with $T_0 = -0.12$ keV. The offset T_0 as found by *Lin and Hoffman, 1979* varied between $+0.05$ keV and $+0.15$ keV. Since the value of T_0 is small in both studies, and since our study shows a different sign than *Lin and Hoffman, 1979*, we adopt the value $T_0 = 0$ in the rest of the paper. Thus we write $T = U/a$ where a is a constant.

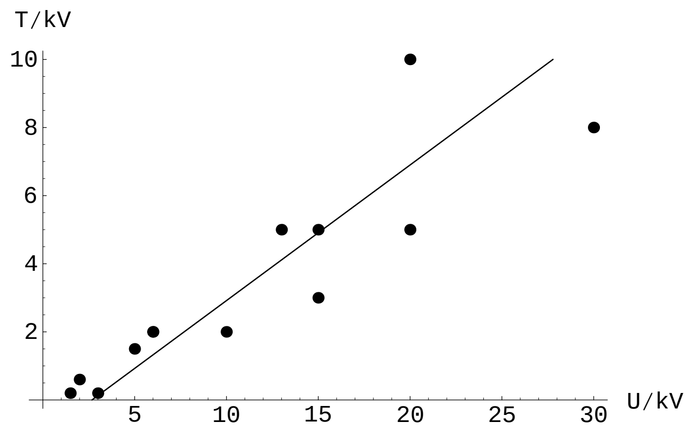

Figure 4. Data points taken from Table 1 of *Olsson et al.* (1998) from nine independent events and different studies where both the thermal energy and the potential drop have been estimated from fitted Maxwellians. The fitted line is $T = -0.12$ keV $+0.31U$.

Considering an O-shaped potential, one has to bear in mind that in the computations underlying Figure 4, a U-shaped potential was always assumed. This does not affect the determination of U from the data, but the determination of T may be affected to some extent. We do not believe this to be a major effect, although we haven't studied it quantitative detail yet. In what follows we will, to simplify notation, use the same value a for both U- and O-shaped potentials. For the U-shaped case $a \approx 3 \pm 1$ is a reasonable estimate, but for the O-shaped case a might be somewhat different, still of the same order of magnitude however.

Assuming $T = U/a$ equation (2.14) becomes

$$j^{M,O}_{\text{Appr.}} = \frac{eN_e}{\sqrt{2\pi m a}} e^{-a}(1+a)\sqrt{U}. \tag{2.15}$$

This is shown in Figure 5 for $a = 3$.

Applying $T = U/a$ in the linear relationship (Equation 10 of *Janhunen and Olsson,* 1998) which is based on the U-shaped potential model we get

$$j^{M,U}_{\text{Appr.}} = \frac{eN_e}{\sqrt{2\pi m a}}(1+a)\sqrt{U}. \tag{2.16}$$

Equation (2.16) is displayed in Figure 6 for $a = 3$. This equation is as the same as the O-shaped result (2.15) but without the factor e^{-a}.

The further approximation $U \gg T$ for which the classical linear current-voltage relationship $j = KV$ (i.e., linear without an offset term) was derived (*Fridman and Lemaire,* 1980, *Knight,* 1973, *Janhunen and Olsson,* 1998) is not very well justifiable since U is typically only about 3 times larger than T.

2.1.2. Maxwellian energy flux. The O-shaped energy flux formula (2.12) for the Maxwellian distribution gives the result

$$\varepsilon^{M,O} =$$

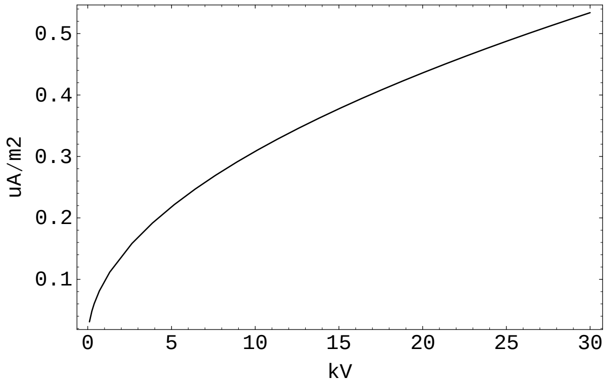

Figure 5. The Maxwellian current-voltage relationship based on the O-shaped potential with the assumption $T = U/a$ where $a = 3$ (equation 2.15). This is a square root relationship. If a smaller value for a was used, the current density would be larger.

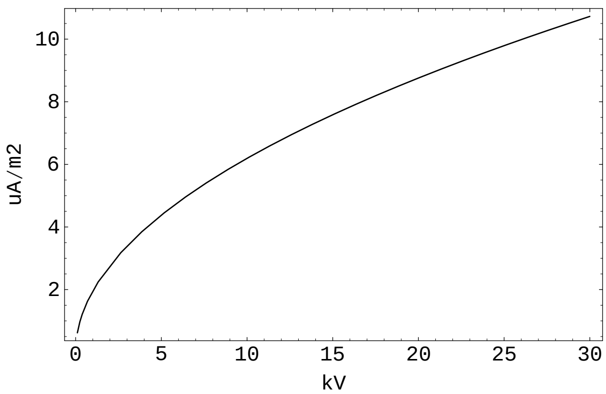

Figure 6. The Maxwellian current-voltage relationship based on the U-shaped potential drop with the assumption $T = U/3$ (equation 2.16). This is again a square root relationship.

$$N_e \frac{e^{-U/T}}{b_o} \sqrt{\frac{T}{2\pi m}} \left[b_i(2T+U) + e^{\frac{b_o U}{(b_o - b_i)T}} \left(2b_o T - b_i(2T+U)\right) \right] \tag{2.17}$$

The approximation for the energy flux yields

$$\varepsilon^{M,O}_{\mathrm{Appr.}} = \exp\left(\frac{-U}{T}\right) \frac{N_e}{\sqrt{2\pi m T}} \left[2T^2 + 2UT + U^2\right] + O\left(b^{-2}\right). \tag{2.18}$$

Applying $T = U/a$ for the approximate energy flux formula (2.18) yields

$$\varepsilon^{M,O}_{\mathrm{Appr.}} = \frac{(2+2a+a^2)N_e e^{-a}}{a^{3/2}\sqrt{2\pi m}} U^{3/2}. \tag{2.19}$$

This result is displayed in Figure 7 for $a = 3$.

Applying $T = U/a$ for the energy flux in the U-shaped case (equation 12 of

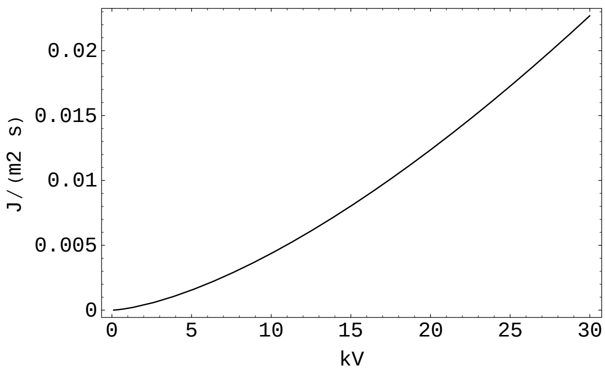

Figure 7. The Maxwellian energy flux based on O-shaped potential with the assumption $T = U/a$ where $a = 3$ (equation 2.19). A smaller numerical value for a would increase the energy flux. The energy flux based on a U-shaped potential also shows a $U^{3/2}$ dependence.

Janhunen and Olsson (1998)) yields

$$\varepsilon^{M,U}_{\text{Appr.}} = \frac{(2 + 2a + a^2)N_e}{a^{3/2}\sqrt{2\pi m}} U^{3/2}. \tag{2.20}$$

which is again the same as the O-shaped result (2.19) but without the factor e^{-a}.

Again, we note that the approximation $U \gg T$ is not very good for the energy flux either. Thus formula 13 of *Janhunen and Olsson* (1998) showing $\varepsilon \sim V^2$ is not very accurate for this reason.

2.2. *Kappa distribution*

We will now derive the exact and approximate current density for the kappa case, where an O-shaped potential is assumed. We will also derive an exact (see Appendix) and approximate kappa energy flux using slightly different methods. We will compare the results with the corresponding formulas for the U-shaped potential.

2.2.1. Kappa current density. For the kappa distribution (2.2) the general current density formula (2.4) yields

$$j^{\kappa,O} = eb_i N_e \sqrt{\frac{T}{2\pi m}}$$
$$\frac{1}{b_o}\left[\left(1 + \frac{U}{\kappa T}\right)^{1-\kappa} + \left(1 + \frac{b_i U}{(b_i - b_o)\kappa T}\right)^{-\kappa}\left(\frac{b_o - 1}{b_i}\right)\left(1 - \frac{b_i U}{(b_o - 1)\kappa T}\right)\right]$$
$$\frac{\Gamma(\kappa + 1)}{\Gamma(\kappa - 1/2)\kappa^{1/2}(\kappa - 1)}. \tag{2.21}$$

When applying the series expansion for $b_i \gg 1$ we get the approximated form

$$j^{\kappa,O}_{\text{Appr.}} =$$

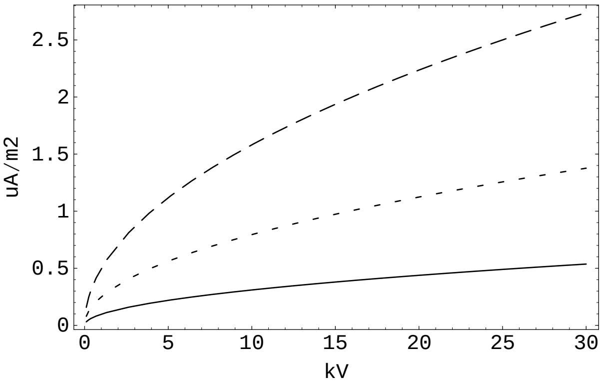

Figure 8. Comparison of different κ values for the approximate kappa current density formula (2.23) for the O-shaped potential. $\kappa = 2$ (dash), $\kappa = 4$ (dot), $\kappa = \infty$ (solid). $T = U/a$ with $a = 3$ has been assumed. A smaller value for a would increase the current density. As seen here, in the O-shaped case the value of κ affects the current density a lot.

$$\frac{eN_e}{\sqrt{2\pi m T}}\left(T + \frac{\kappa-1}{\kappa}U\right) \frac{\Gamma(\kappa+1)}{\Gamma(\kappa-1/2)\kappa^{1/2}(\kappa-1)} \frac{\left(1+\frac{U}{\kappa T}\right)^{-\kappa}}{1-\frac{U}{\kappa(T+U)}}. \tag{2.22}$$

We apply $T = U/a$ in equation (2.22) and get

$$j^{\kappa,O}_{\text{Appr.}} = \frac{eN_e(1+a)\left(1+\frac{a}{\kappa}\right)^{-\kappa}\Gamma(\kappa+1)}{(\kappa-1)\sqrt{2\pi m\kappa a}\,\Gamma(\kappa-1/2)}\sqrt{U}. \tag{2.23}$$

This equation is plotted for varying κ for $a = 3$ in Figure 8. The current depends rather strongly on the value of κ in the O-shaped case.

Applying $T = U/a$ for the U-shaped potential drop formula (equation 15 of *Janhunen and Olsson* (1998)) we obtain

$$j^{\kappa,U}_{\text{Appr.}} = \frac{eN_e\left(1+\frac{a(\kappa-1)}{\kappa}\right)\Gamma(\kappa+1)}{(\kappa-1)\sqrt{2\pi m\kappa a}\,\Gamma(\kappa-1/2).}\sqrt{U} \tag{2.24}$$

This has been plotted for varying κ for $a = 3$ in Figure 9. It is seen that the dependence on the values of κ is only slight in the U-shaped case.

2.2.2. Kappa energy flux. As is the case with the U-shaped potential (*Janhunen and Olsson,* 1998), it seems to be difficult to to compute the exact energy flux for the kappa distribution by the direct method (equation 2.12). In the Appendix we present another exact method that works in both U- and O-shaped cases. However, here we are mostly interested in the approximate result in the limit $b_i \gg 1$, and we derive it by going back to (2.11) and (2.12). In the limit $b_i \gg 1$, the first integrals in equations (2.11) and (2.12) are of order $O(b_i^{-2})$ and can be dropped. After some

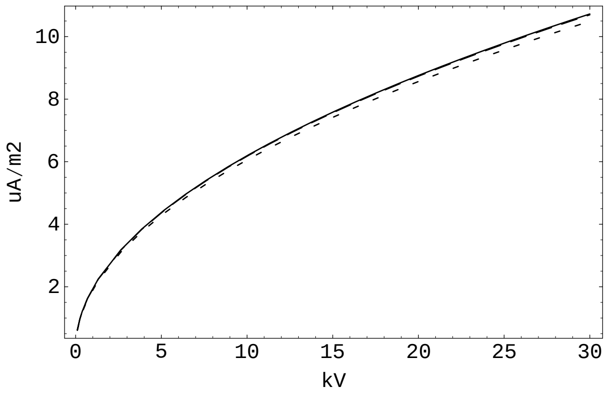

Figure 9. Comparison of different κ values for the approximate kappa current density formula for the U-shaped potential (equation 2.24). $\kappa = 2$ (dash), $\kappa = 4$ (dot), $\kappa = \infty$ (solid). $T = U/3$ has been used. The dependence on κ is only slight.

manipulations we obtain

$$j^O = \frac{2\pi e}{m^2} \int_{U(b_o)}^{\infty} dW_\parallel f(W_\parallel, 0) W_\parallel + O\left(\frac{1}{b_i}\right) \tag{2.25}$$

$$\varepsilon^O = \frac{2\pi}{m^2} \int_{U(b_o)}^{\infty} dW_\parallel f(W_\parallel, 0) W_\parallel^2 + O\left(\frac{1}{b_i}\right) \tag{2.26}$$

In the U-shaped case a corresponding result is given by equation 18 in *Janhunen and Olsson* (1998). The U-shaped results can also be written in the form

$$j^U = \frac{2\pi e}{m^2} \int_0^{\infty} dW_\parallel f(W_\parallel, 0)(W_\parallel + eV) + O\left(\frac{1}{b_i}\right) \tag{2.27}$$

$$\varepsilon^U = \frac{2\pi}{m^2} \int_0^{\infty} dW_\parallel f(W_\parallel, 0)(W_\parallel + eV)^2 + O\left(\frac{1}{b_i}\right) \tag{2.28}$$

which clearly reveals the physical difference between the O-shaped and U-shaped potentials: In the U-shaped case there is a net potential difference between the source plasma and the ionosphere and therefore the term eV must be added. In the O-shaped case there is no such term, but instead the integration domain is reduced because low energy particles are reflected back by the O-shaped potential.

The application of (2.26) to the kappa distribution yields

$$\varepsilon^{\kappa,O}_{\text{Appr.}} = \frac{N_e \Gamma(\kappa+1)}{\sqrt{2\pi\kappa m T}\,\Gamma(\kappa - 1/2)} \left(1 + \frac{U}{\kappa T}\right)^{-\kappa} \left[\frac{2\kappa T^2 + 2\kappa T U + (\kappa-1)U^2}{(\kappa-1)(\kappa-2)}\right]. \tag{2.29}$$

Substituting $T = U/a$ yields

$$\varepsilon^{\kappa,O}_{\text{Appr.}} = \frac{N_e \Gamma(\kappa+1)}{\sqrt{2\pi\kappa m}\,\Gamma(\kappa - 1/2)} \left(1 + \frac{a}{\kappa}\right)^{-\kappa} \left[\frac{a^2(\kappa-1) + 2(a+1)\kappa}{a^{3/2}(\kappa-1)(\kappa-2)}\right] U^{3/2}. \tag{2.30}$$

Equation (2.30) is plotted for varying κ for $a = 3$ in Figure (10). The energy flux

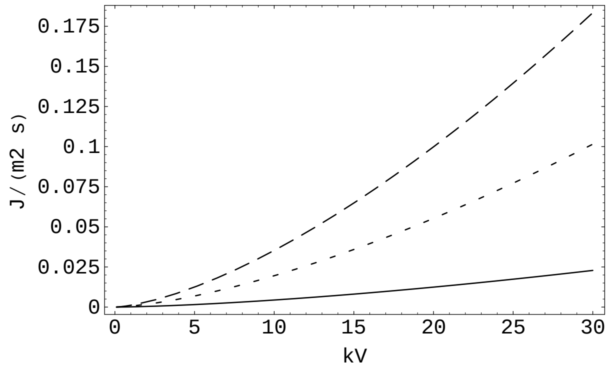

Figure 10. Comparison of different κ values for the approximate kappa energy flux formula for the O-shaped potential. $\kappa = 3$ (dash), $\kappa = 4$ (dot), $\kappa = \infty$ (solid). $T = U/a$ with $a = 3$ has been assumed. A smaller value for a would increase the energy flux.

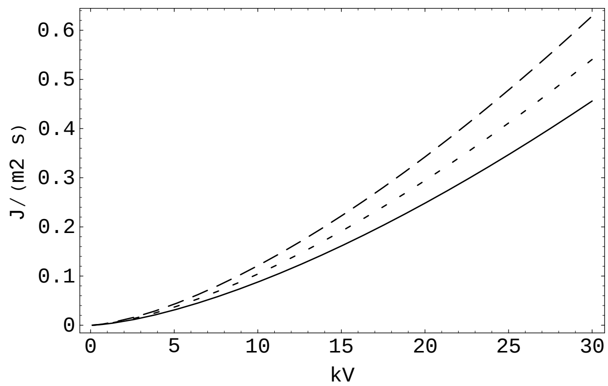

Figure 11. Comparison of different κ values for the approximate kappa energy flux formula for the U-shaped potential with $T = U/3$. $\kappa = 3$ (dash), $\kappa = 4$ (dot), $\kappa = \infty$ (solid).

depends rather strongly on the value of κ, as was the case for the O-shaped current density also.

Applying $T = U/a$ for the approximate U-shaped kappa energy flux formula [equation 19 of *Janhunen and Olsson* (1998)] gives

$$\varepsilon_{\text{Appr.}}^{\kappa,U} = \frac{N_e \Gamma(\kappa+1)}{\sqrt{2\pi\kappa m}\,\Gamma(\kappa-1/2)} \left[\frac{2a(\kappa-2)\kappa + 2\kappa^2 + a^2(2-3\kappa-\kappa^2)}{a^{3/2}\kappa(\kappa-1)(\kappa-2)} \right] U^{3/2}. \quad (2.31)$$

This has been plotted for $a = 3$ in Figure (11).

3. Physical implications

In all figures thus far shown, a has been assumed to be the same ($a = 3$) in both U- and O-shaped cases, which gives rather low values for the current density in the

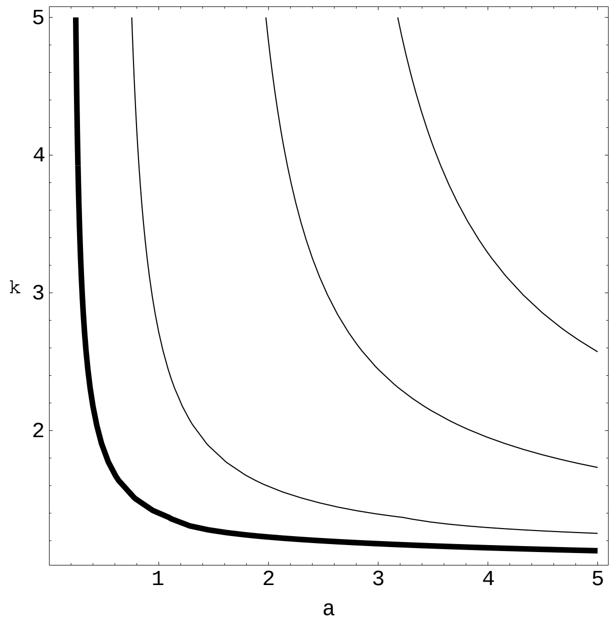

Figure 12. Values of a and κ which for the O-shaped case give the same current density ($\sim 0.6\mu$ A m^{-2}) as the U-shaped case gives for $a = 3$ and $\kappa = \infty$ (i.e. Maxwellian). The thick curve represents the case where the source plasma density N_e in the O-shaped case has the same value as in the U-shaped case (0.1 cm^{-3}). The other curves from left to right correspond to cases where the O-shaped N_e is higher by factors of 2, 5 and 10, respectively. The potential U is 10 kV.

O-shaped case. Lowering a (i.e., increasing T, $T = U/a$) increases the O-shaped current density.

It was also seen that the value of κ does not have much effect in the U-shaped case, but does change the current a lot in the O-shaped case. Lowering κ increases the O-shaped current density significantly because then there is larger number of higher energy particles and only those particles with higher energy than the potential barrier carry a current in the O-shaped case.

Observations indicate (*Olsson et al.,* 1996, *Olsson et al.,* 1998) that the source plasma densities deduced from low-altitude observations by assuming a U-shaped potential tend to be somewhat smaller than what we would expect in this region of the magnetosphere. Previously we have invoked an incomplete loss cone filling during one bounce period as a possible explanation (*Olsson and Janhunen,* 1998). An O-shaped potential filters out the low-energy part of the magnetospheric population, thus reducing the precipitating current and making the low-altitude N_e look smaller (i.e., look smaller if the data are analyzed using a U-shaped interpretation as it has been done in all previous studies). The O-shaped potential could be an alternative explanation for the relatively low source plasma densities. Thus it makes sense to consider what happens if the parameter N_e in the O-shaped case has a higher value than in the U-shaped case.

In Figure 12 we show four curves for four different O-shaped source plasma densities. Each curve gives the combination of O-shaped a and κ parameters which give the same current ($\sim$ 0.6μ A m^{-2}) as a U-shaped model would give, with $a = 3$ and $\kappa = \infty$. From the figure we can see all the effects discussed in the above

O-shaped	U-shaped
$j^M = e^{-a}\frac{eN_e(1+a)}{\sqrt{2\pi ma}}\sqrt{U}$	$j^M = \frac{eN_e(1+a)}{\sqrt{2\pi ma}}\sqrt{U} = 0.92\frac{eN_e}{\sqrt{m}}\sqrt{U}$
$\varepsilon^M = e^{-a}\frac{eN_e(2+2a+a^2)}{a^{3/2}\sqrt{2\pi m}}U^{3/2}$	$\varepsilon^M = \frac{eN_e(2+2a+a^2)}{a^{3/2}\sqrt{2\pi m}}U^{3/2} = 3.27\frac{eN_e}{\sqrt{2\pi m}}U^{3/2}$
$j^\kappa = \frac{eN_e(1+a)\left(1+\frac{a}{\kappa}\right)^{-\kappa}\Gamma(\kappa+1)}{\sqrt{2\pi ma\kappa}(\kappa-1)\Gamma(\kappa-1/2)}\sqrt{U}$	$j^\kappa = \frac{eN_e\left(1+a-\frac{a}{\kappa}\right)\Gamma(\kappa+1)}{\sqrt{2\pi ma\kappa}(\kappa-1)\Gamma(\kappa-1/2)}\sqrt{U}$
$\varepsilon^\kappa = \frac{N_e\Gamma(\kappa+1)\left(1+\frac{a}{\kappa}\right)^{-\kappa}(a^2(\kappa-1)+2(a+1)\kappa)}{\sqrt{2\pi\kappa m}\Gamma(\kappa-1/2)a^{3/2}(\kappa-1)(\kappa-2)}U^{3/2}$	$\varepsilon^\kappa = \frac{N_e\Gamma(\kappa+1)(2a(\kappa-2)\kappa+2\kappa^2+a^2(2-3\kappa-\kappa^2))}{\sqrt{2\pi\kappa m}\Gamma(\kappa-1/2)a^{3/2}\kappa(\kappa-1)(\kappa-2)}U^{3/2}$

Table 1. Summary of the approximate formulas in O-shaped and U-shaped potentials for Maxwellian and kappa distributions, where $T = U/a$ has been assumed. The numerical values in the U-shaped case were obtained by assuming $a = 3$.

paragraphs quantitatively: the O-shaped current is smaller than the U-shaped one for the same parameters, but lowering either a or κ or increasing N_e can make the currents equal. Values of a smaller than unity are not very sensible because then the temperature would be larger than the peak energy. Likewise, values of κ less than two are questionable since the energy flux becomes divergent then. For example, a reasonable position in the figure might be $a = 1.5, \kappa \approx 2$ and N_e multiplied by 2. However, a real numerical value of a has to be found from a statistical study where T, U are estimated from fittings in observed spectra of low-orbiting satellite differential electron flux data.

4. Summary of results

We computed the current density and energy flux for the case when precipitating auroral electrons go through an O-shaped potential. They are derived for both Maxwellian and kappa distributions. Both exacts formula and approximations are derived. The approximations are almost generally valid and uses only $B(src) \ll B(i)$. We applied $T = U/a$ (where the default of $a = 3$ is used in the U-shaped model) to the formulas. We compared these formulas with those based on the U-shaped potential which were derived earlier (*Janhunen and Olsson,* 1998).

The resulting formulas in each case are summarized in Table 1. The parameter N_e here is equal to the true magnetospheric electron density multiplied by the loss cone filling rate (see below for an explanation of the loss cone filling rate). Notice that in the case of an O-shaped model the density of magnetospheric electrons observed at low altitudes can be significantly smaller than N_e because the low-energy particles are filtered out by the O-shaped potential barrier.

We summarize our new findings briefly.

(a) In all cases the approximated current density and energy flux is almost indistinguishable from the exact formula. This was not shown in the figures, but it was checked anyway.

(b) Previous statistical studies show that the source plasma temperature T and the peak energy U are related by $T = U/a$ where a is around 3 in the U-shaped potential model. The numerical value of a has to be estimated from a statistical study for the O-shaped model.

(c) Since a is not very large, it is not a very good approximation to drop the offset term from the linearized Knight formula. Thus, $j = KV$ is a rather questionable formula even if the U-shaped potential is valid.

(*d*) In both O-shaped and U-shaped cases the current density becomes proportional to $\sqrt{U}$ and the energy flux to $U^{3/2}$, if $T = U/a$ is assumed.

(*e*) In the O-shaped case the current density and energy flux depend much more strongly on the value of κ than in the U-shaped case.

(*f*) Making a smaller, κ smaller or N_e larger increases the current and energy flux in the O-shaped model.

(*g*) The kappa distribution can be expressed as a superposition of Maxwellians, which gives a new analytic method for deriving kappa results directly from Maxwellian results. Using this technique it is possible to derive the exact kappa energy fluxes (see Appendix).

Appendix. Kappa as a superposition of Maxwellians

In this Appendix we show how to express the kappa distribution as a superposition (integral) of Maxwellians. Because source plasma particle contributes to the current and energy flux linearly, we can use this method to generate kappa results from existing Maxwellian ones directly. Using this method it is possible to derive the exact kappa energy fluxes for both U- and O-shaped potentials, which we did not succeed in doing by the direct method (equations 2.11 and 2.12).

In this Appendix we define

$$f_M(W,T) = N_e \left(\frac{m}{2\pi T}\right)^{3/2} e^{-W/T} \tag{A 1}$$

for the isotropic Maxwellian and

$$f_\kappa(W,T,\kappa) = N_e \left(\frac{m}{2\pi\kappa T}\right)^{3/2} \frac{\Gamma(\kappa+1)}{\Gamma(\kappa-1/2)} \left(1+\frac{W}{\kappa T}\right)^{-\kappa-1} \tag{A 2}$$

for the kappa distribution. An integral relationship

$$f_\kappa(W,T,\kappa) = \int_0^\infty K(\kappa,T,T_1) f_M(W,T_1) dT_1 \tag{A 3}$$

where

$$K(\kappa,T,T_1) = \frac{\kappa T \left(\frac{\kappa T}{T_1}\right)^{\kappa-3/2} e^{-\kappa T/T_1}}{T_1^2 \Gamma(\kappa-1/2)} \tag{A 4}$$

now exists between these distributions as can be seen rather easily.

To compute a kappa formula from a corresponding Maxwellian one, one replaces T by T_1 in the Maxwellian result, multiplies it by $K(\kappa,T,T_1)$ and integrates over T_1. The method is very general, it works for all quantities that obey the superposition principle. Physically speaking, the kappa distribution has been written as a weighted average of many Maxwellian populations, which all contribute to the precipitating fluxes.

To demonstrate the power of this method we now derive the exact kappa energy flux formula for the O-shaped potential by starting from (2.17). The result is

$$\varepsilon^{\kappa,O} = N_e \sqrt{\frac{T}{2\pi m}} \frac{1}{b_o} \left(1 + \frac{U}{\kappa T}\right)^{1-\kappa} \left[\frac{\kappa^{3/2}\Gamma(\kappa-1)}{(\kappa-2)\Gamma(\kappa-1/2)}\right] \left\{ b_i(2T+U) + [2b_oT - b_i(2T+U)] \times \left[1 + \frac{b_oU}{(b_i-b_o)(\kappa T+U)}\right]^{1-\kappa} \right\}. \tag{A 5}$$

We checked that equation (A 5), when developed to first order in $1/b_i$, gives equation (2.29).

As a second example we derive the corresponding U-shaped result, using equation 9 of *Janhunen and Olsson,* 1998 and using that paper's notation ($U = eV$, $x = 1/(b_i-1)$, $b_i = B_i/B_m$):

$$\varepsilon^{\kappa,U} = N_e \left(\frac{B_i}{B_m}\right) \sqrt{\frac{T}{2\pi m}} \left[\frac{\kappa^{3/2}\Gamma(\kappa-1)}{(\kappa-2)\Gamma(\kappa-1/2)}\right] \left\{ 2T + U\left(1 - \frac{2}{\kappa}\right) - \left(1 + \frac{xeV}{\kappa T}\right)^{1-\kappa} \times \left[T + \frac{T}{1+x} + U\left((1+x)\left(1-\tfrac{1}{\kappa}\right) - \frac{1}{\kappa(1+x)}\right)\right]\right\}. \tag{A 6}$$

This is a new result that we were not able to derive in *Janhunen and Olsson,* 1998.

Finally we note that equation (9) of *Janhunen and Olsson,* 1998 contains an unfortunate printing error: the factor $T_\perp + eV(1 + x(T_\perp/T_\parallel))$ appearing in that formula should be divided by $1 + x$.

References

Bryant, D.A., Electron acceleration in the aurora and beyond, Institute of Physics Publishing, Bristol, 1999.

Carlqvist, P. and R. Boström, Space-charge regions above the aurora, *J. Geophys. Res., 75,* 7140–7146, 1970.

Collier, M.R., The adiabatic transport of superthermal distributions modelled by kappa functions, *Geophys. Res. Lett., 22,* 2673–2676, 1995.

Fridman, M., and J. Lemaire, Relationship between auroral electron fluxes and field aligned electric potential differences, *J. Geophys. Res. 85*, 664-670, 1980.

Janhunen, P., GUMICS-3 — a global ionosphere-magnetosphere coupling simulation with high ionospheric resolution, *Proc. of ESA 1996 symposium on environment* *modelling for space-based applications,* ESA/ESTEC, 18-20 Sep., 1996, ESA SP-392, 1996.

Janhunen, P., and A. Olsson, The current-voltage relationship revisited: exact and approximate formulas with almost general validity for hot magnetospheric electrons for bi-Maxwellian and kappa distributions, *Ann. Geophys., 16,* 292–297, 1998

Janhunen, P., A. Olsson, F.S. Mozer and H. Laakso, How does the U-shaped potential close above the acceleration region? A study using Polar data, *Ann. Geophys., in press,* 1999.

Knight, S., Parallel electric fields, *Planet. Space Sci. 21*, 741-750, 1973.

Lemaire, J. and Scherer, M., Plasma sheet particle precipitation: A kinetic model, *Planet. Space Sci. 21,* 281–289, 1973.

Lemaire, J. and Scherer, M., Field aligned distribution of plasma mantle and ionospheric plasmas, *J. Atmos. Terr. Phys. 40,* 337–342, 1978.

Lemaire, J. and Scherer, M., Field-aligned current density versus electric potential characteristics for magnetospheric flux tubes, *Ann. Geophys. 1,* 91-96, 1983.

Lin, C.S, and R.A. Hoffman, Characteristics of the inverted-V event, *J. Geophys. Res., 84,* 1514-1525, 1979.

Lundin, R., and I. Sandahl, Some characteristics of the parallel electric field acceleration of electrons over discrete auroral arcs as observed from two rocket flights, *ESA SP-135*, 125-136, 1978.

Olsson, A., A.I. Eriksson and P. Janhunen, On the current-voltage relationship in auroral breakups and westwards-travelling surges, *Ann. Geophys., 14,* 1265–1273, 1996.

Olsson, A. and P. Janhunen, A case study of electron precipitation in the late substorm growth phase on and nearby a preonset arc, *Ann. Geophysicae,* in press, 1998.

Olsson, A., Andersson, L., Eriksson, A.I., Clemmons, J., Erlandsson, R.E., Reeves, G., Hughes, T. and Murphree, J.S., Freja studies of the current-voltage relation in substorm related events, *J. Geophys. Res.,* 103, 4285–4301, 1998.

Vasyliunas, V.M., A survey of low-energy electrons in the evening sector of the magnetosphere with OGO1 and OGO3, *J. Geophys. Res., 73,* 2839–2884, 1968.